FE Modeling of Strain Localization in Soft Rock

By Ronaldo I. Borja,[1] Richard A. Regueiro,[2] and Timothy Y. Lai[3]

Abstract: A finite-element (FE) model of localized deformation in soft rock taking a strong discontinuity approach is presented. The model is formulated within the context of rate-independent, nonassociated Drucker-Prager plasticity with nonlinear cohesion hardening/softening. Strain localization is modeled as a jump in the displacement field and simulated within the framework of the FE method using the standard Galerkin approximation. The model is used to simulate the load-displacement behavior of Gosford sandstone deforming in plane strain, focusing on the prediction of the stress levels necessary to initiate strain localization, based on the strong and weak discontinuity criteria (jumps in displacement and strain, respectively), and on the demonstration of mesh-independence of the FE solutions in the bifurcated state. For the sandstone, the onset of weak discontinuity is detected first, before the onset of strong discontinuity, suggesting a possible coupling of the two types of discontinuities in the strain-softening regime.

INTRODUCTION

Strain localization is a ubiquitous feature of geologic materials undergoing nonhomogeneous deformation. In rocks, the zone of localized deformation is generally referred to as either a fault, shear band, rupture zone, or simply a failure plane, and is best explained by either fracture mechanics (Horii and Nemat-Nasser 1982; Ashby and Hallam 1986) or bifurcation theory (Rudnicki and Rice 1975). Localized deformation is typically followed by a reduction in overall strength of the material body as loading proceeds (Read and Hegemier 1984). It is therefore of considerable interest and importance to be able to predict when a shear band forms and how this narrow zone of discontinuity is oriented within the rock material.

Much experimental work has been conducted to understand the inception of localized deformation in soil and rock by relating the microscopic behavior (e.g., microcracking in brittle rocks, mineral particle rolling and sliding in granular soils, and mineral particle rotation and translation in the cement matrix of soft rocks such as sandstone) to the macroscopic behavior via overall load-displacement curves (Santarelli and Brown 1989; Wawersik et al. 1990; Ord et al. 1991; Borja and Wren 1995a,b; Labuz et al. 1996; Wren and Borja 1997; Borja et al. 1998). This paper does not focus on this microscopic-macroscopic connection but instead attempts to numerically model localized deformation from the macroscopic standpoint. To this end, we use the finite-element (FE) method and present a model that is objective with respect to mesh refinement and insensitive to mesh alignment. We then use this model to predict the onset of localization in frictional materials exemplified by soft rocks and trace the orientation and progression of the shear bands, including the subsequent softening response following strain localization.

Various approaches have been proposed to circumvent the problem of mesh dependence in FE modeling of strain localization phenomena: length-scale incorporated in the plastic evolution equations (Pietruszczak and Mróz 1981); nonlocal approach (Bazant and Pijaudier-Cabot 1988; Adachi et al. 1991); adaptive remeshing (Zienkiewicz et al. 1995); the weak discontinuity approach (Rudnicki 1977; Ortiz et al. 1987); element breaking (Wan et al. 1990); and the strong discontinuity approach (Larsson et al. 1993; Simo et al. 1993; Armero and Garikipati 1995; Regueiro et al. 1998; Regueiro and Borja 1999; Borja and Regueiro 2000). This paper takes the strong discontinuity approach to model localized deformation in frictional materials. The approach relies on the hypothesis of a discontinuous displacement field, which naturally leads to a shear band of zero thickness. In particular, we will use the model by Borja (2000), Borja and Regueiro (2000), and Regueiro and Borja (1999, 2000) for computational modeling of shear band formation in soft rocks. This model is formulated within the context of nonassociated Drucker-Prager plasticity and lately has been implemented within the framework of the standard Galerkin approximation (Borja 2000). The resulting model is demonstrably objective with respect to mesh refinement and insensitive to mesh alignment.

Plane strain-stress conditions are most commonly encountered in geotechnical engineering. However, plane strain compression tests of soft rocks, herein defined as rocks with unconfined compressive strengths below 35 MPa (Labuz and Papamichos 1991), are uncommon because of the limitation of existing laboratory testing apparatus. Essential features of plane strain compression apparatus for rocks include either a stiff frame design or more expensive hydraulic active systems and the absence of kinematic constraints that inhibit the free formation of a shear band on the plane of loading. Quite recently, some high-quality test results from plane strain compression tests of soft rocks have been reported in the literature (Labuz and Papamichos 1991; Ord et al. 1991; Yumlu and Ozbay 1995; Labuz et al. 1996). In this paper, we will use the compression test results reported by Ord et al. (1991) for Gosford sandstone to illustrate the capabilities of the model to simulate the localization phenomena in a plane strain setting.

LOCALIZATION MODEL

Typical behavior of rocks subjected to monotonic uniaxial compression can be summarized with the aid of the stress-strain curve shown in Fig. 1. The stress-strain curve divides into four regions (Jaeger and Cook 1976): (1) *OA*, in which it is slightly concave upwards; (2) *AB*, a nearly linear portion; (3) *BC*, in which it is concave downwards, reaching a maximum at *C*; and (4) a falling region *CD*. In the first two regions, *OA* and *AB*, the behavior is very nearly elastic, while in the third region *BC*, irreversible plastic deformations are induced in the rock. The region *CD* is characteristic of brittle behavior, but this portion is usually obscured by the instability of the machine-specimen system after violent failure very near to the point *C*. A similar description may be made of the stress-strain curve for rocks subjected to a positive confining pressure, with

[1]Assoc. Prof., Dept. of Civ. and Envir. Engrg., Terman Engrg. Ctr., Stanford Univ., Stanford, CA 94305-4020.

[2]Grad. Student, Dept. of Civ. and Envir. Engrg., Stanford Univ., Stanford, CA.

[3]Grad. Student, Dept. of Civ. and Envir. Engrg., Stanford Univ., Stanford, CA.

Note. Discussion open until September 1, 2000. To extend the closing date one month, a written request must be filed with the ASCE Manager of Journals. The manuscript for this paper was submitted for review and possible publication on June 1, 1998. This paper is part of the ***Journal of Geotechnical and Geoenvironmental Engineering***, Vol. 126, No. 4, April, 2000. ©ASCE, ISSN 1090-0241/00/0004-0335–0343/$8.00 + $.50 per page. Paper No. 18473.

the additional feature that the failure strength at point *C* tends to increase as the confining pressure increases (Handin 1966).

Rocks generally exhibit a compactive behavior during the initial portion of the stress-strain curve, but throughout much of the plastic region *BC*, and especially the rest of the falling region *CD*, they exhibit pervasive dilatancy as open microcracks form within the rock specimens (Brace et al. 1966; Cook 1970). This implies an increase in volume during compression relative to the behavior of a linear, elastic material. This typical volume change behavior is shown in Fig. 2. There is sufficient evidence that dilatant behavior also manifests in plane strain-stress conditions and is not restricted to the uniaxial or biaxial stress cases alone (Ord et al. 1991; Yumlu and Ozbay 1995).

Motivated by these observations, we now turn to the modeling aspect and illustrate the role of the proposed localization model in interpreting the stress-strain responses of soft rock specimens deforming in plane strain. Although the theory is quite general, we will consider a more specific nonassociated Drucker-Prager plasticity model to interpret the experimental responses of these materials. In the Drucker-Prager plasticity model, the yield surface is a right circular cone in principal stress space and contains the elastic region represented by portions *OA* and *AB* of the stress-strain curve shown in Fig. 1. At initial yield denoted by point *B*, the yield surface hardens by allowing the cohesion to increase nonlinearly with effective plastic strain up until point *C*. This type of hardening is termed ''cohesion hardening'' by Vermeer and de Borst (1984). Somewhere near point *C*, the specimen undergoes strain localization

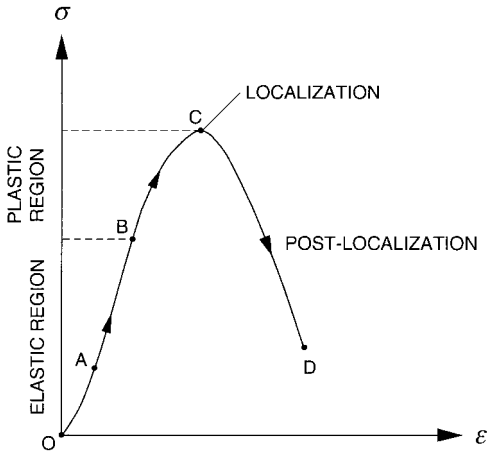

FIG. 1. Typical Stress-Strain Curve for Rock under Uniaxial Compression (after Jaeger and Cook 1976)

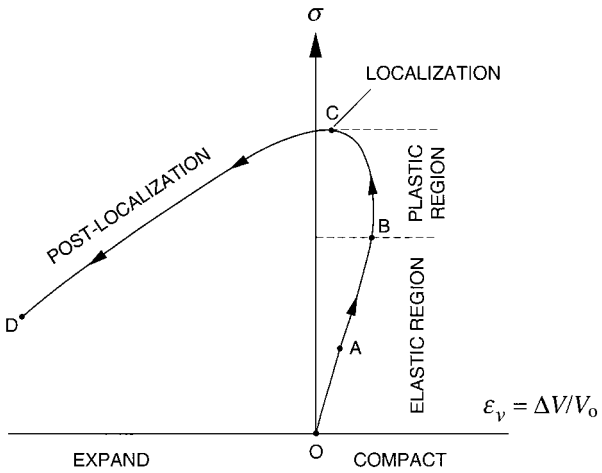

FIG. 2. Typical Axial Stress–Volumetric Strain Curve for Rock under Uniaxial Compression (after Jaeger and Cook 1976)

predicted by a localization condition, and so a jump in the displacement field is introduced to capture the discontinuity or slip along the shear band.

The following section presents the continuum and discrete versions of the proposed localization model. To provide a reference point of view for subsequent discussion, a weak discontinuity type of formulation is first briefly summarized. Then, the proposed strong discontinuity type of formulation is presented and compared with the weak discontinuity model. For a more rigorous mathematical treatment of the strong discontinuity model applied to cohesive/frictional material, the reader is referred to Borja and Regueiro (2000) and Borja (2000).

Weak Discontinuity Formulation

Let us consider an initially homogeneously deforming elastoplastic continuum defined by a yield function F and a plastic potential function Q. The rate-constitutive equation for this continuum is given by

$$\dot{\sigma}_{ij} = c^{ep}_{ijkl}\dot{\varepsilon}_{kl} \tag{1}$$

where $\dot{\sigma}_{ij}$ = Cauchy stress rate tensor; $\dot{\varepsilon}_{kl}$ = small strain rate tensor; and c^{ep}_{ijkl} = rank-four elastoplastic tangential moduli tensor given explicitly by the well-known expression

$$c^{ep}_{ijkl} = c^{e}_{ijkl} - \frac{1}{\chi}\left(c^{e}_{ijpq}\frac{\partial Q}{\partial \sigma_{pq}}\frac{\partial F}{\partial \sigma_{rs}}c^{e}_{rskl}\right); \quad \chi = \frac{\partial F}{\partial \sigma_{ij}}c^{e}_{ijkl}\frac{\partial Q}{\partial \sigma_{kl}} + H \tag{2}$$

in which c^{e}_{ijkl} = rank-four elastic moduli tensor; and H = plastic modulus. Throughout this paper, the Einstein convention is used for repeated indices.

The idea in the classical weak discontinuity type of formulation is to consider the occurrence of a jump in the strain field across a certain narrow zone of intense straining, called shear band (Rudnicki and Rice 1975). Thus, the total strain inside the shear band is equal to the homogeneous strain outside the shear band plus a jump in the strain field represented by the symmetric component of the dyadic tensor $g_k n_l$, where g_k = element of the jump vector **g**, and n_l = element of unit vector **n** perpendicular to the shear band. Since the equations of continuing equilibrium require that the traction vector outside the shear band be equal to the traction vector inside the shear band, then

$$n_i c^{ep}_{ijkl}\dot{\varepsilon}^{*}_{kl} = n_i c^{ep}_{ijkl}[\dot{\varepsilon}^{*}_{kl} + \mathrm{sym}(g_k n_l)] \tag{3}$$

where $\dot{\varepsilon}^{*}_{kl}$ is the homogeneous strain field just outside the shear band; and ''sym'' denotes the symmetric component of a tensor. For a nontrivial solution $g_k \neq 0$ to exist, we require that

$$\det(n_i c^{ep}_{ijkl} n_l) = \det(a^{ep}_{jk}) = 0 \tag{4}$$

where a^{ep}_{jk} is the elastoplastic acoustic tensor. Eq. (4) is a necessary condition for the onset of a jump discontinuity in the strain field and states that for some orientation **n**, a jump in the strain field is possible, provided that the determinant of the acoustic tensor vanishes for this particular orientation. A well-known problem with the weak discontinuity formulation, however, lies in the difficult characterization of the response following the emergence of the shear band, since conventional rate-independent elastoplastic models do not provide a characteristic length scale to allow continuation of the solution beyond the point of localization.

Strong Discontinuity Formulation

Let us consider the same elastoplastic continuum described in the previous section, but now assume a jump discontinuity in the displacement field **u** of the form

$$\mathbf{u} = \bar{\mathbf{u}} + [\mathbf{u}]H_{\mathcal{S}}(\mathbf{x}); \quad H_{\mathcal{S}}(\mathbf{x}) = \begin{cases} 1 & \text{if } \mathbf{x} \in \Omega_+ \\ 0 & \text{if } \mathbf{x} \in \Omega_- \end{cases} \tag{5}$$

where $H_{\mathcal{S}}$ = Heaviside function, $\bar{\mathbf{u}}$ = continuous part of $\mathbf{u}$ and $[u]$ = displacement jump discontinuity on the surface $\mathcal{S}$ separating the subdomains Ω_+ and Ω_- of an initially continuous body Ω (Fig. 3). The associated total strain rate tensor resulting from this discontinuous displacement field is the symmetric component of the displacement gradient tensor, which can be written in compact form as (Simo et al. 1993)

$$\dot{\varepsilon}_{kl} = \dot{\varepsilon}^{*}_{kl} + \text{sym}([\dot{u}_k]n_l)\delta_{\mathcal{S}} \tag{6}$$

where $\dot{\varepsilon}^{*}_{kl} = \text{sym}(\partial\dot{\bar{u}}_k/\partial x_l)$ = nonsingular part of $\dot{\varepsilon}_{kl}$; $[\dot{\mathbf{u}}]$ = velocity jump vector; n_k = element of unit vector $\mathbf{n}$ perpendicular to the surface $\mathcal{S}$ and pointing in the direction of Ω_+; and $\delta_{\mathcal{S}}$ = Dirac delta function on the surface $\mathcal{S}$. The deformation described by (5) has the physical significance that the zone of intense shearing has a characteristic thickness of zero.

The rate-constitutive equation for the continuum is given by

$$\dot{\sigma}_{ij} = c^{e}_{ijkl}\left[\dot{\varepsilon}^{*}_{kl} + \text{sym}([\dot{u}_k]n_l)\delta_{\mathcal{S}} - \lambda\frac{\partial Q}{\partial \sigma_{kl}}\right] \tag{7}$$

Now, since the stresses are bounded, (7) will be meaningful only if the consistency parameter λ takes the form $\lambda = \lambda_\delta\delta_{\mathcal{S}}$, where $\lambda_\delta > 0$ is a real number, which implies that plasticity is concentrated to the surface of discontinuity (Simo et al. 1993). Under this condition, the equations of continuing equilibrium require that the traction vector outside the band be equal to the traction vector inside the band, or

$$n_i c^{e}_{ijkl}\dot{\varepsilon}^{*}_{kl} = n_i c^{e}_{ijkl}\dot{\varepsilon}^{*}_{kl} + n_i C^{ep}\,\text{sym}([\dot{u}_k]n_l)\delta_{\mathcal{S}} \tag{8}$$

where C^{ep}_{ijkl} = elastic–perfectly plastic tangential moduli tensor given by the expression

$$C^{ep}_{ijkl} = c^{e}_{ijkl} - \frac{1}{X}\left(c^{e}_{ijpq}\frac{\partial Q}{\partial\sigma_{pq}}\frac{\partial F}{\partial\sigma_{rs}}c^{e}_{rskl}\right); \quad X = \frac{\partial F}{\partial\sigma_{ij}}c^{e}_{ijkl}\frac{\partial Q}{\partial\sigma_{kl}} \tag{9}$$

For a nontrivial solution $[\dot{u}_k] \neq 0$ to exist, we require that

$$\det(n_i C^{ep}_{ijkl} n_l) = \det(A^{ep}_{jk}) = 0 \tag{10}$$

where A^{ep}_{jk} = elastic–perfectly plastic acoustic tensor. Eq. (10) is a necessary condition for the emergence of a jump discontinuity in the displacement field and has a meaning analogous to but not the same as the condition for the emergence of a jump discontinuity in the strain field.

A comparison between conditions (4) and (10) is in order. First, since $\chi \neq X$ unless $H = 0$ for the case of perfect plasticity, then $a_{jk} \neq A_{jk}$, and so conditions (4) and (10) generally occur at two different states of stress. Furthermore, since c^{e}_{ijkl} is positive-definite, and

$$a_{jk} = a^{e}_{jk} - a^{p}_{jk}; \quad A_{jk} = A^{e}_{jk} - A^{p}_{jk} \tag{11}$$

where $a^{e}_{jk} = n_i c^{e}_{ijkl} n_k$, etc., then both $\det(a_{jk})$ and $\det(A_{jk})$ approach zero from the positive side (Runesson et al. 1991).

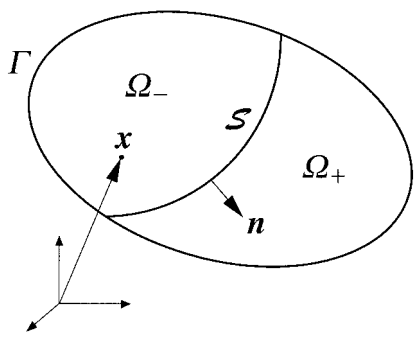

FIG. 3. Definition of Surface of Discontinuity

Therefore, it follows that if localization takes place in the hardening regime where $H > 0$ (which is possible for the case of nonassociated plasticity), then the onset of displacement jump will theoretically precede the onset of strain jump. Conversely, if localization takes place in the softening regime where $H < 0$, then the onset of strain jump will precede the onset of displacement jump. Finally, it must be noted that, although the localization condition for the emergence of a displacement discontinuity does not explicitly contain the continuum plastic modulus H, the determinant expression (10) is still a function of the stress state, which in turn depends on the value of the plastic modulus used to predict that particular stress state, and so the determinant expression for predicting the onset of displacement jump is not completely independent of H.

Model for Bifurcated Response

The main reason for advocating the strong discontinuity formulation in this paper is that this approach allows continuation of the solution beyond the point of bifurcation. However, a key point to remember in modeling the bifurcated response is that, once the element has localized, both the continuum yield and plastic potential functions are replaced by a different set of yield and plastic potential functions reflecting the constitutive response of the damaged element due to yielding on the band. It is therefore important to formulate an appropriate damage model that captures the bifurcated response of the material. To this end, let us consider a damage model defined by a yield function G of the form

$$G = \text{sym}(n_i t_j)\sigma_{ij} - [c - (n_i n_j)\sigma_{ij}\tan\phi] = 0 \tag{12}$$

where t_j = component of unit vector $\mathbf{t}$ tangent to the band; c = cohesion intercept; and ϕ = mobilized friction angle developed on the surface of discontinuity. Eq. (12) has the physical significance that yielding on the band occurs when the resolved tangential shear stress reaches a certain maximum value, and that this maximum value varies linearly with the normal component of the compressive stress acting on the slip surface. If $\phi = 0$, then we recover a yield criterion analogous to crystal plasticity theory in which the shear band corresponds to a potential crystallographic slip plane (Borja and Wren 1992, 1993).

Similarly, the kinematics of strong discontinuity presented in (5) may be assumed at postlocalization, leading to a rate-constitutive equation of the form analogous to (7) as

$$\dot{\sigma}_{ij} = c^{e}_{ijkl}\left[\dot{\varepsilon}^{*}_{kl} + \dot{\zeta}\,\text{sym}(m_k n_l)\delta_{\mathcal{S}} - \lambda\frac{\partial R}{\partial\sigma_{kl}}\right] \tag{13}$$

where $\dot{\zeta}$ = magnitude of the jump rate vector $[\dot{u}_k]$; m_k = component of unit vector in the direction of the jump rate vector; and R = plastic potential function in the damaged state. As before, we require that $\lambda = \lambda_\delta\delta_{\mathcal{S}}$, since the stresses must be bounded, which in turn results in the flow rule for the slip tensor of the form

$$\dot{\zeta}\,\text{sym}(m_k n_l) = \lambda_\delta\frac{\partial R}{\partial\sigma_{kl}} \Rightarrow \frac{\partial R}{\partial\sigma_{kl}} \propto \text{sym}(m_k n_l) \tag{14}$$

Eq. (14) guarantees that the stresses are bounded everywhere, even on the band, and allows the shear band to evolve in the bifurcated state.

It is useful to compare the gradient tensors derived from the yield function G and the plastic potential function R, since together they describe the response of the continuum in the damaged state. Taking the stress gradient of G from (12) gives

$$\frac{\partial G}{\partial\sigma_{kl}} \propto \text{sym}(\mu_k n_l); \quad \mu_k = t_k + n_k\tan\phi \tag{15}$$

For planar deformation, Fig. 4(a) shows how this gradient tensor is constructed from the unit normal vector $\mathbf{n}$ and the vector $\boldsymbol{\mu}$ (note that $\|\boldsymbol{\mu}\| = \sqrt{1 + \tan^2\phi} \neq 1$, unless $\phi = 0$). The vector $\boldsymbol{\mu} = \mathbf{t} + \mathbf{n} \tan \phi$ is seen to make an angle of ϕ relative to the surface of discontinuity. In contrast, Fig. 4(b) shows that the slip tensor is constructed from the unit vectors $\mathbf{n}$ and $\mathbf{m}$, where the latter vector makes an angle of ψ relative to the band and defines the instantaneous direction of the displacement jump increment. If the mobilized friction angle ϕ is equal to the dilation angle ψ, then the two gradient tensors are parallel and the flow rule is associative at postlocalization. However, this is generally not the case since ψ is determined from the bifurcation analysis whereas ϕ is a prescribed parameter defining the postlocalization constitutive response.

Continued yielding on the band is possible provided that the damage model satisfies the consistency condition

$$\dot{G} = \text{sym}(\mu_i n_j) c^e_{ijkl} \left[\dot{\varepsilon}^*_{kl} + \dot{\zeta}\, \text{sym}(m_k n_l) \delta_{\mathcal{S}} - \lambda \frac{\partial R}{\partial \sigma_{kl}} \right] - H\lambda = 0 \tag{16}$$

where H = softening modulus in the damaged state. Following the same argument used in the previous section, we conclude that since $\lambda = \lambda_\delta \delta_{\mathcal{S}}$, then $H^{-1} = H_\delta^{-1} \delta_{\mathcal{S}}$, where $H_\delta < 0$ is the softening modulus on the band, i.e., both λ and H must be treated as singular distributions (Stakgold 1998). Thus, the consistency condition reduces to

$$\text{sym}(\mu_i n_j) c^e_{ijkl} \dot{\varepsilon}^*_{kl} - H_\delta \lambda_\delta = 0 \tag{17}$$

Alternately, since $\dot{\zeta} \propto \lambda_\delta$ from the flow rule (14), then a softening modulus $\tilde{H}_\delta = H_\delta \lambda_\delta / \dot{\zeta} < 0$ may be defined on the band, in which case the consistency condition (17) can be written in the alternative form (Borja and Regueiro 2000)

$$\text{sym}(\mu_i n_j) c^e_{ijkl} \dot{\varepsilon}^*_{kl} - \tilde{H}_\delta \dot{\zeta} = 0 \tag{18}$$

where $\dot{\zeta}$ = magnitude of the slip rate.

The model described above has been implemented into a FE code using the standard Galerkin formulation (Borja 2000). For the case of piecewise constant stress interpolation, the standard Galerkin approximation has been shown to be equivalent to the assumed enhanced strain FE approximation presented by Borja and Regueiro (2000) and leads to a solution for the bifurcated response that is independent of mesh refinement and insensitive to mesh alignment. The following section describes how the model is used to interpret the mechanical behavior of a soft rock subjected to plane strain compression. The simulations include prediction of the onset of localization and the evolution of the shear band. For simplicity, we restrict the development to quasi-static problems under the assumption of infinitesimal deformation. Furthermore, only plane strain deformation is considered, and discussion is restricted to constant-strain triangular (CST) elements.

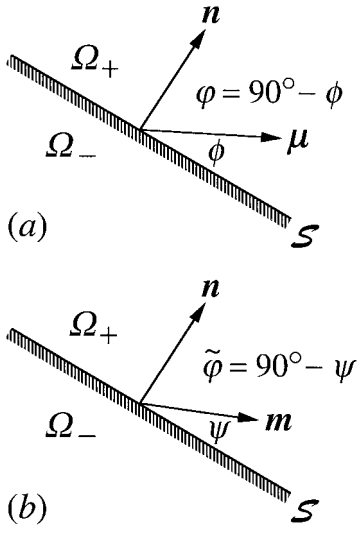

FIG. 4. Construction of Gradient Tensors: (a) Gradient of Yield Function *G*; (b) Gradient of Plastic Potential *R*

NUMERICAL SIMULATIONS

In this section we will use the proposed model to simulate the behavior of a soft rock under plane strain compression, focusing on the experiments on Gosford sandstone described by Ord et al. (1991). The goal of the simulations is not to demonstrate that the model provides accurate predictions of the load-displacement responses per se, but to show how the model may be used to interpret the stress-strain behavior exhibited by the rock specimens within the context of the localization phenomena. In fact, the idea of the simulations is precisely to provide the model the flexibility to capture the stress-strain responses exhibited by the rock specimens as closely as possible, identify the instant at which the model predicts the formation of a shear band, and then use these results to infer the cause of the softening response exhibited by the rock specimens. Obviously, the simulations will necessitate a specific form of the constitutive model and the assumption of the material parameter values; it turns out that, for the sandstone examples, we can sufficiently constrain the boundary value problem to allow the model to generate meaningful solutions.

For the constitutive model in the prelocalization regime, we assume a nonassociated Drucker-Prager plasticity theory with cohesion hardening/softening (Borja and Regueiro 2000). Here, the yield function F and its gradient with respect to σ_{ij} take the form

$$F = \sqrt{\frac{3}{2} s_{ij} s_{ij}} - \sqrt{3}(\alpha - \beta_p) = 0; \quad \frac{\partial F}{\partial \sigma_{ij}} = \sqrt{\frac{3}{2}} \hat{n}_{ij} + \frac{1}{\sqrt{3}} \beta \delta_{ij} \tag{19}$$

where α, β = model parameters; $p = \sigma_{kk}/3$ = mean normal stress; $\hat{n}_{ij} = s_{ij} / \sqrt{s_{kl} s_{kl}}$; $s_{ij} = \sigma_{ij} = p\delta_{ij}$ = deviatoric component of σ_{ij}; and δ_{ij} = Kronecker delta. The plastic potential function Q is assumed to have a stress gradient of the form

$$\frac{\partial Q}{\partial \sigma_{ij}} = \sqrt{\frac{3}{2}} \hat{n}_{ij} + \frac{1}{\sqrt{3}} b \delta_{ij} \tag{20}$$

where b = dilatancy parameter. Clearly, $b = \beta$ implies associated plasticity.

The procedure followed in the analyses goes as follows. First, we construct different FE meshes for the rock specimens deforming homogeneously. Requiring the meshes to deform homogeneously ensures that all of the elements will satisfy the localization criterion at the same time, and that the initiation of the bifurcated response will take place at the same stress state regardless of the mesh. No weak element is introduced, and no specific band-tracing algorithm is employed, other than having all the elements on a potential shear band traced simultaneously. For a homogeneously deforming specimen, the bifurcation analysis yields two possible shear band orientations and an infinite number of shear band positions; of these, one of the two orientations is chosen and one shear band position is traced. Although there are an infinite number of possible shear bands, the load-displacement curves generated by the model should be the same, regardless of the shear band chosen, in order for the solution to be meaningful. Indeed, results of the numerical examples demonstrate that this is the case, in addition to all the meshes providing identical results to ma-

chine precision demonstrating mesh-independence of the FE solutions.

Model Parameters for Gosford Sandstone

Gosford sandstone is a medium-grained cemented rock from the larger Triassic Hawkesbury sandstone unit of the Sydney Basin, Australia. The plane strain compression apparatus used in the experiments can accommodate rocks with uniaxial compressive strengths of up to 70 MPa, while allowing spontaneous formation of shear bands in the specimens. The loading area of the specimen is about 80 × 40 mm, and the plane strain surface is also 80 × 40 mm. Figs. 5 and 6 show the specimen dimensions and the FE meshes used in the numerical simulations. The FE meshes shown in Fig. 6 include two regular unstructured meshes of different resolution, in which the elements are defined by regular triangulation (CST) with the element sides not necessarily aligned to the potential shear band, and a completely irregular mesh of CST elements that considers two possible shear band orientations. A higher shear band position is also considered with the regular unstructured mesh. By considering these different meshes, we can demonstrate the objectivity of the solutions with respect to mesh refinement and alignment.

Ord et al. (1991) reported results for 11 experiments, five of which involved rock failure by shear banding (see Table 1 of their paper). Of these five experiments, we will focus our simulation on experiment RAO636, corresponding to a specimen tested at a confining pressure of 20 MPa, and on RAO627, corresponding to a confining pressure of 10 MPa. Like most of the other specimens tested, these two specimens exhibited load-displacement curves that clearly show the four regions of loading defined in Fig. 1.

The measured elastic Young's moduli for the sandstone vary from a low of 12.1 GPa to a high of 18.3 GPa, with values tending to increase with higher confining pressures. As mentioned previously, our approach involves capturing the load-displacement curves as closely as possible, and for experiments RAO636 and RAO627, the best-fit initial tangential moduli to the load displacement curves are provided by values of Young's moduli of E = 17.2 and 10.5 GPa, respectively. The initial, slightly concave elastic portions of the load-displacement curves have been ignored.

Ord et al. (1991) also reported values of Poisson's ratio ν varying from 0.24 to 0.40 for all the sandstone specimens. For experiment RAO636, the specimen has a Poisson's ratio of ν = 0.30, while for experiment RAO627, the specimen has ν = 0.40. These values of E and ν used in the simulations are comparable to those reported by Haas (1981).

The Drucker-Prager parameters α and β were estimated by identifying the point on the experimental stress-strain curve at

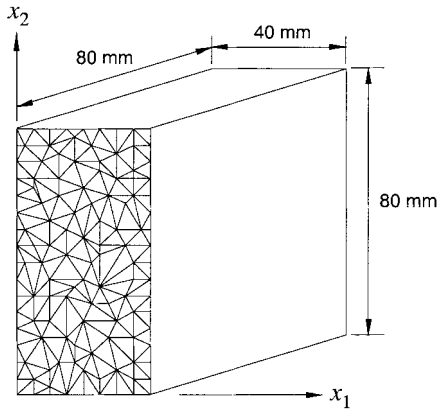

FIG. 5. Rock Specimen Dimensions and Irregular FE Mesh for Sandstone Example

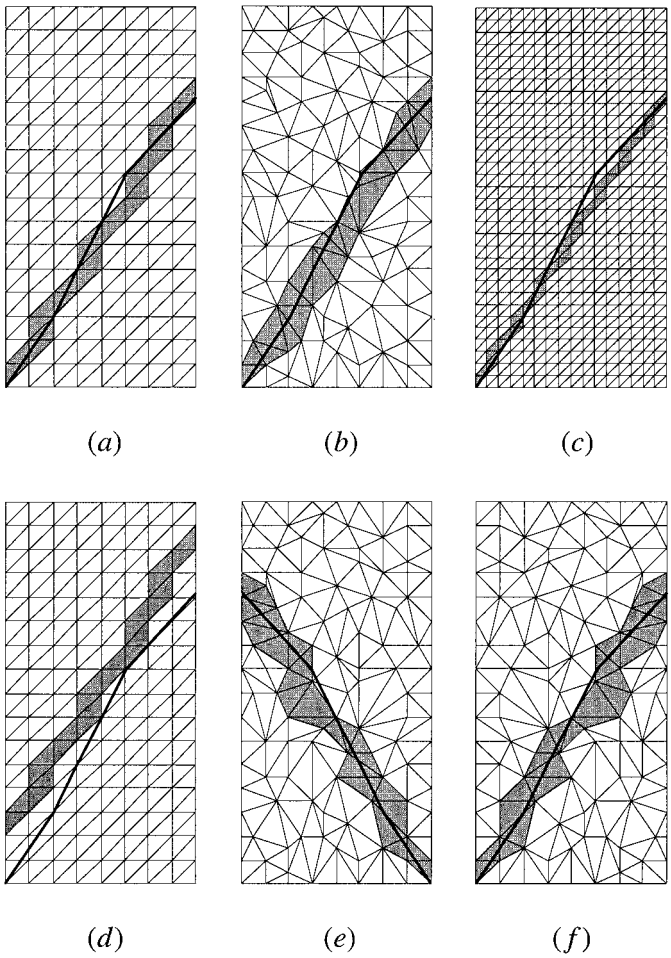

FIG. 6. FE Meshes for Sandstone Example Demonstrating Mesh-Independence of FE Solutions: (a) Regular Unstructured Mesh; (b) Irregular Mesh; (c) Regular Unstructured Finer Mesh; (d) Regular Unstructured Mesh with Higher Band Position; (e) Irregular Mesh with Second Band Orientation; (f) Irregular Mesh Equivalent to (e). Shaded Region Represents Traced Elements while Solid Curve Represents Actual Shear Band on Rock Specimen

which the response begins to deviate from a straight line. A linear regression of the stress-strain curves for the five experiments that resulted in failure by shear banding yields α = 13.5 MPa and β = 0.49. As for the dilatancy parameter b, Ord et al. (1991) reported an average value of the continuum dilatancy angle ψ = 20° prior to peak stress for the intact sandstone; assuming that the dilatancy parameter b varies with the continuum dilatancy angle ψ in the same way that the Drucker-Prager parameter β varies with the continuum friction angle ϕ (Vermeer and de Borst 1984), we obtain b = 0.35 for the sandstone.

All of the Drucker-Prager model parameters have now been determined for the sandstone except for the continuum plastic modulus H, which we will use in the simulations to capture the observed nonlinear load-displacement response. In order to allow the solution to freely capture the nonlinear hardening/softening response, we assume an expression for the plastic modulus H of the form

$$H = H_0 + H_1\gamma^p \geq H_2; \quad \gamma^p = \int_0^t \dot{\gamma}^p \, dt \tag{21}$$

where $\dot{\gamma}^p = (2\dot{e}^p_{ij}\dot{e}^p_{ij}/3)^{1/2}$ = effective deviatoric plastic strain rate; $\dot{e}^p_{ij} = \dot{\varepsilon}^p_{ij} - \dot{\varepsilon}^p_{kk}\delta_{ij}/3$ = deviatoric component of plastic strain rate tensor $\dot{\varepsilon}^p_{ij}$; $H_0 > 0$ is the initial hardening modulus; $H_1 < 0$ is the rate of degradation of H with effective plastic strain; and

$H_2 < 0$ is the softening cutoff parameter introduced to ensure that the quantity χ defined in (2) is always greater than zero. Values of the moduli parameters for the two test problems are reported in the discussions that follow.

Results of Simulations

For experiment RAO636, in which the specimen was subjected to a confining stress of 20 MPa, the values $H_0 = 0.6$ GPa; $H_1 = -125.0$ GPa; and $H_2 = -1.5$ GPa provide a best-fit curve to the nonlinear load-displacement response of the sandstone. The load-displacement curves predicted by the meshes of Fig. 6 are shown in Fig. 7, along with the experimental curve obtained by Ord et al. (1991). The responses predicted by all of the FE meshes are the same, and in fact are all identical to machine precision, demonstrating objectivity of the FE solutions with respect to mesh refinement and insensitivity to mesh alignment. The onset of plasticity is detected at point *A* in Fig. 7, and the plastic modulus H changes in sign well within the rising part of the load-displacement curve at point *B*. That the curve is still rising when H is already negative may be explained from the dependence of the yield function on the mean normal stress. The model detects the onset of weak discontinuity at point *C*, based on the satisfaction of (4), but ignores this aspect of the solution and later detects the onset of strong discontinuity at point *D*, based on the satisfaction of the determinant condition (10). This result agrees with the point made earlier that the onset of weak discontinuity precedes the onset of strong discontinuity when the localization takes place within the region where $H < 0$.

Beyond point *D*, the FE solution is enhanced by introducing a displacement jump mode to capture the accelerated softening response. Fig. 7 shows two such possible postlocalization responses depending on the value of the band softening parameter $\tilde{H}_\delta$. For postlocalization analysis, a value of $\phi = 30°$ was assumed for the mobilized friction angle on the surface of discontinuity [see (12)]. If the displacement jump mode had not been introduced and the specimen had been assumed to deform homogeneously all throughout the simulation, then the load displacement curve predicted by the model would have been as indicated by the dashed curve following point *D* in Fig. 7, and any attempt to make the curve soften faster by decreasing H further would fail since the most negative value of H is bounded by the restriction that the quantity χ in (2) would always be greater than zero. Clearly, the accelerated softening response exhibited by the rock specimen cannot be captured by the standard FE solution unless some kinematical enhancements are introduced.

It is interesting to note that the peak response exhibited by the specimen occurred somewhere between points *C* and *D*, which suggests that there could have been some possible coupling between the emergence of the weak and strong discontinuities, that is, the presence of jump in the strain field could have altered the material response near the band and accelerated the onset of displacement jump. In contrast, this coupling would not likely occur if localization had taken place in the hardening region since, by hypothesis, the material just outside the band would unload elastically upon the onset of strong discontinuity. In the present simulation, the model ignores the presence of weak discontinuity altogether and assumes that the rock specimen remained intact until the onset of strong discontinuity.

Fig. 8 shows the variation of the continuum softening modulus H and the effective plastic strain γ^p with vertical displacement as the rock specimen deforms homogeneously. By allowing the plastic modulus H to vary with γ^p according to (21), the solution was able to determine objectively that the onset of strong discontinuity would occur in the region where H is less than zero. Note, however, that the result of this simulation does not necessarily imply that the onset of strong discontinuity would always occur in the softening region, since localization in the hardening regime is also possible when the plasticity model is nonassociated [see Runesson et al. (1991) and the examples presented by Borja (2000)]. As Fig. 8 indicates, the artificial softening cutoff parameter H_2 did not play a role in the simulation since the onset of strong discontinuity has been detected when H is still above this cutoff value.

Fig. 9 shows the deformed meshes after the enhancements have been introduced in the postlocalization regime, demonstrating a sharp resolution of the discontinuity. Observe the marked dilatancy within the localized elements (shaded gray) exhibited by the FE solutions. The model predicts a shear band orientation of 56.3° relative to the horizontal axis, based on the weak discontinuity criterion (point *C* in Fig. 7) and 57.4° based on the strong discontinuity criterion (point *D* in Fig. 7). The small discrepancy between the two angles is due to the difference in the states of stress at which the two localization conditions have been detected. The corresponding dilatancy angle ψ defining the instantaneous direction of the incremental displacement jump is 22.6° [Fig. 4(b)]. Note that the dilatancy angle ψ is not the same as the continuum dilatancy angle ψ used to define the Drucker-Prager parameter b—the former pertains to the dilatancy angle on the band in the damaged state, whereas the latter pertains to the plastic volumetric response of the intact continuum. Identical load-displacement responses are generated by choosing a higher shear band position, as well as by assuming the second shear band orientation.

It is interesting to see how the shear band orientation at the onset of strong discontinuity is influenced by the parameters

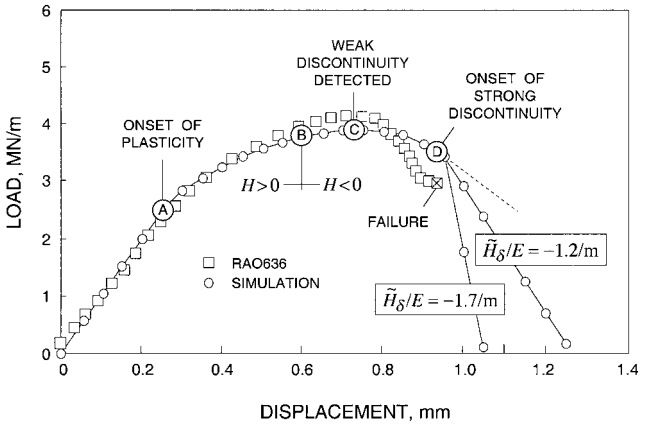

FIG. 7. Load-Displacement Curves for Gosford Sandstone Tested at Confining Stress of 20 MPa

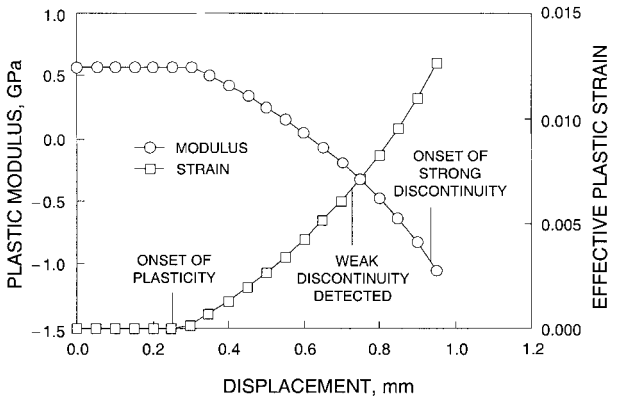

FIG. 8. Variation of Continuum-Effective Plastic Strain and Plastic Modulus with Vertical Displacement: Confining Pressure = 20 MPa

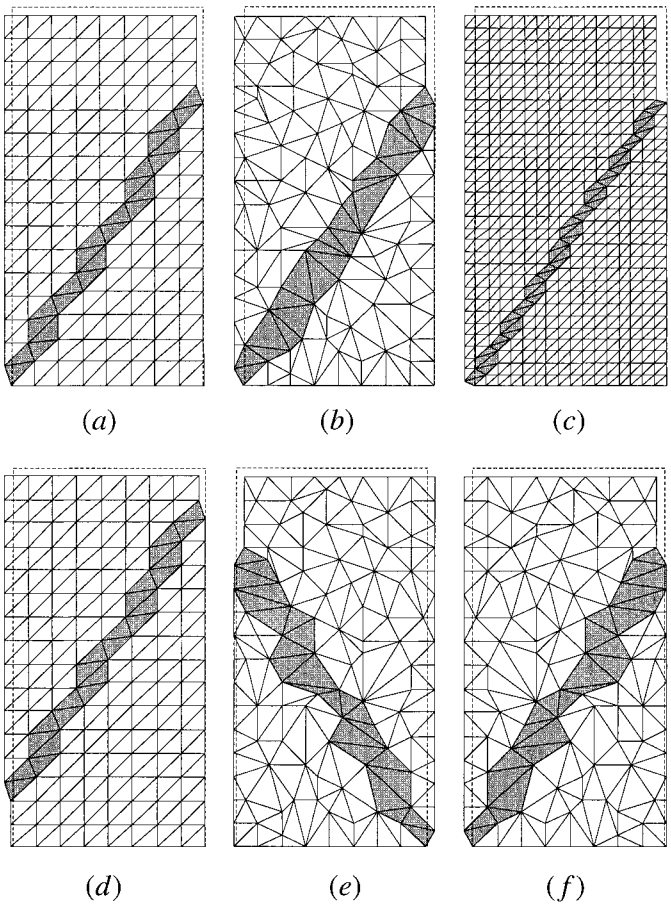

FIG. 9. Deformed Meshes for Sandstone Example Demonstrating Sharp Resolution of Discontinuity: (a) Regular Unstructured Mesh; (b) Irregular Mesh; (c) Regular Unstructured Finer Mesh; (d) Regular Unstructured Mesh with Higher Band Position; (e) Irregular Mesh with Second Band Orientation; (f) Irregular Mesh Equivalent to (e)

β and b of the Drucker-Prager model. Assuming that the parameters β and b are related to the respective continuum friction and dilatancy angles, $\bar{\phi}$ and $\bar{\psi}$, via the relationships

$$\beta = \frac{6 \sin \bar{\phi}}{\sqrt{3}(3 + \sin \bar{\phi})}; \quad b = \frac{6 \sin \bar{\psi}}{\sqrt{3}(3 + \sin \bar{\psi})} \tag{22}$$

then we have $\bar{\phi} = 30°$ and $\bar{\psi} = 20°$, corresponding to the values of β and b used in the simulation. We see that the shear band orientation of 57.4° determined from the localization analysis is closer to the value given by the expression $45° + (\bar{\phi} + \bar{\psi})/4 = 57.5°$, an approximate relationship proposed by Arthur et al. (1977), than to the values provided by either the expression $45° + \bar{\phi}/2 = 60°$ or the expression $45° + \bar{\psi}/2 = 55°$. The actual shear band reported by Ord et al. (1991) for this experiment is sketched in Fig. 6, along with the traced elements (shaded gray) predicted by the FE model.

Fig. 10 superimposes the axial strain–lateral strain curve predicted by the model with the experimental curve for another Gosford sandstone specimen tested by Ord et al. (1991) at a confining pressure of 15 MPa (experiment RAO640). It was not possible to use the corresponding curve for the 20 MPa-confining stress case because the figure reported by Ord et al. for this experiment had no labels; but for rock materials, this small difference in the confining stresses should not have much impact on the volumetric response. For purposes of definition, the predicted axial strain is equal to the axial displacement divided by the original sample height of 80 mm (nominal strain definition), while the lateral strain is equal to the difference in lateral displacements of the two vertical faces of the specimen divided by the original sample width of 40 mm. Note that the sum of the lateral strain and axial strain in this case does not necessarily represent the total volumetric strain at postlocalization when the sample is deforming nonhomogeneously. Observe from the simulation curve that at the onset of yielding, the sample dilates during compression relative to the behavior in the elastic regime. The lateral strains predicted by the model agree well with the experimental values.

For experiment RAO627, in which the specimen was subjected to a confining stress of 10 MPa, the values $H_0 = 0.9$ GPa; $H_1 = -235.0$ GPa; and $H_2 = -1.0$ GPa provide a best-fit curve to the nonlinear load-displacement response of the sandstone. The load-displacement curves predicted by the meshes of Fig. 6 are shown in Fig. 11, along with the experimental curve obtained by Ord et al. (1991). Again, the responses predicted by the three meshes are identical to machine precision, demonstrating mesh-independence of the FE solutions. In this case, the rock specimen fractured to failure almost immediately before a weak discontinuity was detected at point *C* in the softening regime, which again preceded the strong discontinuity detected at point *D*. Also, the material parameters used in the simulation reproduced the experimental curve very well. This latter point should not be construed as an indication of a ''perfect prediction'' since the model parameters have been chosen to match the experimental curve in the first place, but rather as an affirmation that a well-calibrated continuum model can indeed be used to infer the inception of shear banding in this particular sandstone specimen.

Finally, Fig. 12 shows the variations of the continuum plastic modulus and the effective plastic strain with vertical displacement leading to localized deformation. Here, the cutoff softening modulus of $H_2 = -1.0$ GPa was responsible for keeping the numerical solution stable, since without this cutoff parameter, the solution would have diverged on the time interval at which the onset of strong discontinuity had been de-

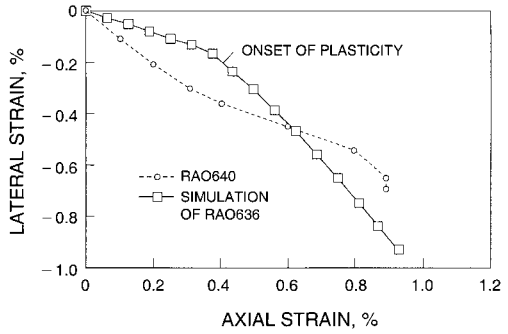

FIG. 10. Axial Strain versus Lateral Strain for Gosford Sandstone

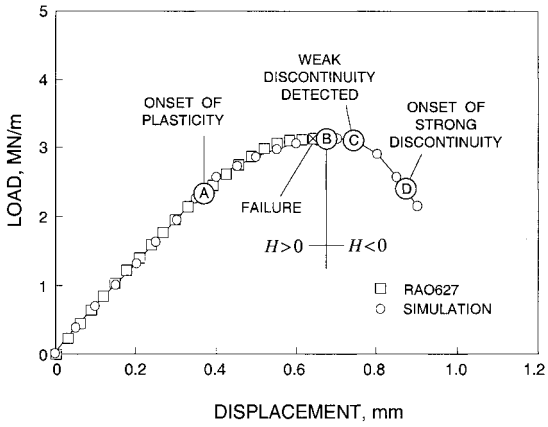

FIG. 11. Load-Displacement Curves for Gosford Sandstone Tested at Confining Stress of 10 MPa

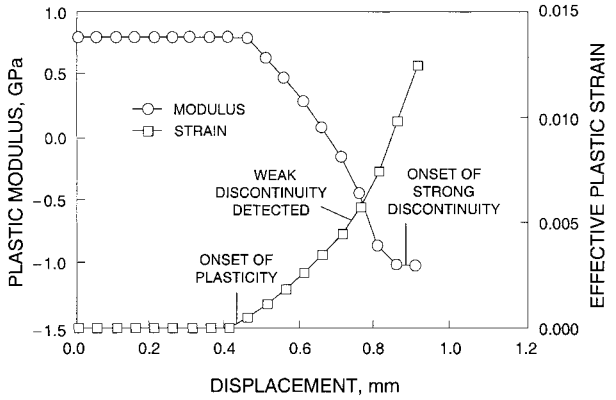

FIG. 12. Variation of Continuum-Effective Plastic Strain and Plastic Modulus with Vertical Displacement: Confining Pressure = 10 MPa

tected. The figure also indicates the satisfaction of both localization criteria in the softening regime where $H < 0$, resulting in the onset of weak discontinuity being detected first before the onset of strong discontinuity.

SUMMARY AND CONCLUSIONS

A finite-element model of localized deformation in soft rock taking a strong discontinuity approach has been presented. The model is formulated within the context of rate-independent, nonassociated Drucker-Prager plasticity with cohesion hardening/softening. Strain localization is modeled as a jump in the displacement field and simulated within the framework of the finite-element method using the standard Galerkin formulation. The model is used to simulate the load-displacement behavior of Gosford sandstone specimens deforming in plane strain. By closely following the experimental load-displacement curves, it is possible to predict the onset of localized deformation in the rock specimens. For the case studies considered in this paper, the onset of weak discontinuity has been detected first, prior to the onset of strong discontinuity, which could suggest a possible coupling of the two types of discontinuities in the strain-softening regime. Further research is under way to study the evolution of the shear bands resulting from the coupling of these two types of discontinuities in the strain-softening regime.

ACKNOWLEDGMENTS

Financial support for this research was provided by the G3S division of the National Science Foundation under contract no. CMS-9700426, through the program of Dr. Priscilla P. Nelson. The writers gratefully acknowledge this support.

APPENDIX. REFERENCES

Adachi, T., Oka, F., and Yashima, A. (1991). ''A finite element analysis of strain localization for soft rock using a constitutive equation with strain softening.'' *Arch. Appl. Mech.*, 61, 183–191.

Armero, F., and Garikipati, K. (1995). ''Recent advances in the analysis and numerical simulation of strain localization in inelastic solids.'' *Proc., Computational Plasticity IV*, D. R. J. Owen, E. Oñate, and E. Hinton, eds., International Center for Numerical Methods in Engineering (CIMNE), Barcelona, Spain, 547–561.

Arthur, J. R. F., Dunstan, T., Al-ani, Q. A. L. J., and Assadi, A. (1977). ''Plastic deformation and failure in granular media.'' *Géotechnique*, London, 27, 53–74.

Ashby, M. F., and Hallam, S. D. (1986). ''The failure of brittle solids containing small cracks under compressive stress states.'' *Acta Metallurgica*, 16, 497–510.

Bazant, Z. P., and Pijaudier-Cabot, G. (1988). ''Nonlocal continuum damage, localization instability and convergence.'' *J. Appl. Mech.*, 55, 287–293.

Borja, R. I. (2000). ''A finite element model for strain localization analysis of strongly discontinuous fields based on standard Galerkin approximation.'' *Comput. Methods Appl. Mech. Engrg.* (in press).

Borja, R. I., and Regueiro, R. A. (2000). ''Strain localization in frictional materials exhibiting displacement jumps.'' *Comput. Methods Appl. Mech. Engrg.* (in press).

Borja, R. I., and Wren, J. R. (1993). ''Discrete micromechanics of elastoplastic crystals.'' *Int. J. Numer. Methods in Engrg.*, Chickester, England, 36(22), 3815–3840.

Borja, R. I., and Wren, J. R. (1995a). ''Micromechanics of continuum models for granular materials.'' *Engrg. Mech., Proc., 10th Conf.*, S. Sture, ed., Vol. 1, ASCE, New York, 497–500.

Borja, R. I., and Wren, J. R. (1995b). ''Micromechanics of granular media, Part I: Generation of overall constitutive equation for assemblies of circular disks.'' *Comput. Methods Appl. Mech. Engrg.*, 127, 13–36.

Borja, R. I., and Wren, J. R. (1992). ''On the bifurcation of elasto-plastic crystals during multiple slip.'' *Engrg. Mech., Proc., 9th Conf.*, L. D. Lutes and J. M. Niedzwecki, eds., ASCE, New York, 284–287.

Borja, R. I., Wren, J. R., and Regueiro, R. A. (1998). ''Micromechanical basis of continuum models for granular media.'' *Localization and bifurcation theory for soils and rocks*, T. Adachi, F. Oka, and A. Yashima, eds., Balkema, Rotterdam, The Netherlands, 295–304.

Brace, W. F., Paulding, B. W., and Scholtz, C. (1966). ''Dilatancy in the fracture of crystalline rocks.'' *J. Geophys. Res.*, 77, 3939.

Cook, N. G. W. (1970). ''An experiment proving that dilatancy is a pervasive volumetric property of brittle rock loaded to failure.'' *Rock Mech.*, 2, 181–188.

Haas, C. J. (1981). ''Chapter 6: Stress-strain relationships.'' *Phys. properties of rocks and minerals*, Vol. II-2, Y. S. Touloukian et al., eds., McGraw-Hill/CINDAS Data Series on Material Properties, New York.

Handin, J. (1966). ''Strength and ductility.'' *Handbook of physical constants*, S. P. Clark, Jr., ed., *Geol. Soc. Am. Memoir*, 97, 223–289.

Horii, H., and Nemat-Nasser, S. (1985). ''Compression-induced microcrack growth in brittle solids: Axial splitting and shear failure.'' *J. Geophys. Res.*, 90, 3105–3215.

Jaeger, J. C., and Cook, N. G. W. (1976). *Fundamentals of rock mechanics*, 2nd Ed., Chapman and Hall, London.

Labuz, J. F., Dai, S. T., and Papamichos, E. (1996). ''Plane-strain compression of rock-like materials.'' *Int. J. Rock Mech. Mining Sci. and Geomech. Abstracts*, Amsterdam, 33, 573–584.

Labuz, J. F., and Papamichos, E. (1991). ''Preliminary results of plane-strain testing of soft rock.'' *Rock mechanics as a multidisciplinary science*, J.-C. Roegiers, ed., Balkema, Rotterdam, The Netherlands, 667–674.

Larsson, R., Runesson, K., and Ottosen, N. S. (1993). ''Discontinuous displacement approximation for capturing plastic localization.'' *Int. J. Numer. Methods in Engrg.*, Chichester, England, 36, 2087–2105.

Ord, A., Vardoulakis, I., and Kajewski, R. (1991). ''Shear band formation in Gosford sandstone.'' *Int. J. Rock Mining Sci. and Geomech. Abstracts*, Amsterdam, 28(5), 397–409.

Ortiz, M., Leroy, Y., and Needleman, A. (1987). ''A finite element method for localized failure analysis.'' *Comput. Methods Appl. Mech. Engrg.*, 61, 189–214.

Pietruszczak, S. T., and Mróz, Z. (1981). ''Finite element analysis of deformation of strain-softening materials.'' *Int. J. Numer. Methods in Engrg.*, Chichester, England, 17, 327–334.

Read, H. E., and Hegemier, G. A. (1984). ''Strain softening of rock, soil and concrete—A review article.'' *Mech. Mat.*, 3, 271–294.

Regueiro, R. A., and Borja, R. I. (1999). ''A finite element model of localized deformation in frictional materials taking a strong discontinuity approach.'' *Finite Elements in Anal. and Des.*, 33(4), 283–315.

Regueiro, R. A., and Borja, R. I. (2000). ''Plane strain finite element analysis of pressure-sensitive plasticity with strong discontinuity.'' *Int. J. Solids Struct.* (in press).

Regueiro, R. A., Lai, T. Y., and Borja, R. I. (1998). ''Computational modeling of strain localization in soft rock.'' *Geotechnics of hard soils–soft rocks*, A. Evangelista and L. Picarelli, eds., Balkema, Rotterdam, The Netherlands, 789–797.

Rudnicki, J. W. (1977). ''The inception of faulting in a rock mass with a weakened zone.'' *J. Geophys. Res.*, 82(5), 844–854.

Rudnicki, J. W., and Rice, J. R. (1975). ''Conditions for the localization of deformation in pressure-sensitive dilatant materials.'' *J. Mech. Phys. Solids*, 23, 371–394.

Runesson, K., Peric, D., and Sture, S. (1991). ''Discontinuous bifurcations of elastic-plastic solutions at plane stress and plane strain.'' *Int. J. Plasticity*, 7, 99–121.

Santarelli, F. J., and Brown, E. T. (1989). ''Failure of three rocks in triaxial and hollow cylinder compression tests.'' *Int. J. Rock Mech. Mining Sci. and Geomech. Abstracts*, Amsterdam, 26, 401–413.

Simo, J. C., Oliver, J., and Armero, F. (1993). ''An analysis of strong

discontinuities induced by strain-softening in rate-independent inelastic solids.'' *Computational Mech.*, 12, 277–296.
Stakgold, I. (1998). *Green's functions and boundary value problems*, 2nd Ed., Wiley, New York.
Vermeer, P. A., and de Borst, R. (1984). ''Nonassociated plasticity for soils, concrete, and rock.'' *Heron*, 29(3), 1–64.
Wan, R. G., Chan, D. H., and Morgenstern, N. R. (1990). ''A finite element method for the analysis of shear bands in geomaterials.'' *Finite Element Anal. Des.*, 7, 129–143.
Wawersik, W. R., Rudnicki, J. W., Olsson, W. A., Holcomb, D. J., and Chau, K. T. (1990). ''Localization of deformation in brittle rock: Theoretical and laboratory investigations.'' S. P. Shah, S. E. Swartz, and M. L. Wang, eds., *Micromechanics of failure of quasi-brittle materials*, Elsevier, New York, 115–124.
Wren, J. R., and Borja, R. I. (1997). ''Micromechanics of granular media, Part II: Overall tangential moduli and localization model for periodic assemblies of circular disks.'' *Comput. Methods Appl. Mech. Engrg.*, 141, 221–246.
Yumlu, M., and Ozbay, M. U. (1995). ''A study of the behaviour of brittle rocks under plane strain and triaxial loading conditions.'' *Int. J. Rock Mech. Min. Sci. and Geomech. Abstracts*, Amsterdam, 32, 725–733.
Zienkiewicz, O. C., Pastor, M., and Huang, M. (1995). ''Softening, localisation and adaptive remeshing: Capture of discontinuous solutions.'' *Computational Mech.*, 17, 98–106.